



## Stable operating windows for polythiophene organic electrochemical transistors

**Scott T. Keene**<sup>1</sup>, Electrical Engineering Division, Department of Engineering, University of Cambridge, Cambridge CB3 0FA, UK; Cavendish Laboratory, Department of Physics, University of Cambridge, Cambridge CB3 0HE, UK

**Luke W. Gatecliff, and Sophia L. Bidinger**, Electrical Engineering Division, Department of Engineering, University of Cambridge, Cambridge CB3 0FA, UK

**Maximilian Moser, and Iain McCulloch**, Department of Chemistry, University of Oxford, Oxford OX1 3TA, UK

**George G. Malliaras**, Electrical Engineering Division, Department of Engineering, University of Cambridge, Cambridge CB3 0FA, UK

Address all correspondence to Scott T. Keene at [stk30@cam.ac.uk](mailto:stk30@cam.ac.uk)

(Received 10 October 2023; accepted 12 December 2023; published online: 29 December 2023)

### Abstract

Organic electrochemical transistors (OECTs) have emerged as a promising platform for biosensing, electrophysiology, and neuromorphic devices. However, OECTs are often limited by the stability of the channel materials. Here, we systematically investigate the stability of OECT channels under varied operating voltage ranges. We find that OECT materials can be operated with high stability when the voltage range is reduced. We show that repeated full voltage cycling degrades device performance. The results indicate that to maximize stability, OECTs should either be operated in the saturation regime to maximize current gain (transconductance) or in the subthreshold regime to maximize the on/off ratio.

### Introduction

Organic electrochemical transistors (OECTs) have recently gained attention for electrophysiology,<sup>[1]</sup> biosensing,<sup>[2]</sup> and neuromorphic devices.<sup>[3]</sup> OECTs are well suited for bioelectronic applications due to their low voltage operation ( $<1$  V), high gain as characterized by their transconductance ( $g_m$ ), and ability to integrate with aqueous and living systems.<sup>[4,5]</sup> OECTs use organic mixed ionic-electronic conductors (OMIECs) as the transistor channel, leveraging the reversible doping of the channel by shuttling ions from an external electrolyte into or out of the bulk material.<sup>[6]</sup>

One often overlooked characteristic of OECT-based technologies is their stability. In biosensing, it is not possible to acquire accurate measurements without strong current stability due to the need to resolve small changes in current.<sup>[7,8]</sup> This current stability is especially relevant when considering that the physiological range of many analytes is significantly narrower than those tested with novel technologies. Likewise, in neuromorphic devices, stability is important as synaptic weights are encoded in the conductance of OECT channels.<sup>[9]</sup> If the conductance decays with each read or write operation, the weights would deviate from their intended values, degrading the accuracy of the network.<sup>[10]</sup> Complementary logic introduces additional complexity as there is dependence on the stability of both the p- and n-type subunits with often highly unbalanced duty cycles.<sup>[11,12]</sup> Degradation of either channel will result in

fluctuations in the switching threshold which could degrade the logic performance or gain.

The reported causes of instability can broadly be divided into two categories: degradation via parasitic electrochemical reactions and disruption of the OMIEC microstructure. Electrochemical degradation is dominated by the presence of hydroxide radicals generated when the OECT channel is fully reduced.<sup>[13]</sup> The concentration of such radicals is increased as a result of oxygen reduction reactions (ORRs) which limits the range of applied voltages over which stable operation can be achieved.<sup>[14]</sup> Microstructural degradation is observed when solvated ions are injected into the film causing both reversible and irreversible swelling.<sup>[15]</sup> It has been shown that when a film is excessively doped this swelling can cause irreversible changes in the crystallinity of the film, reducing the conductivity.<sup>[16]</sup>

Several stability-improving strategies have been explored which aim to prevent instabilities caused by either of these mechanisms. Electrochemical degradation is often avoided by suppressing ORRs either by changing the energy levels of the system or blocking molecular oxygen from reaching the OMIEC channel. Previously reported energetic methods include modification of the polymer structure to change the ionization potential<sup>[14]</sup> suppressing the peroxide forming ORR or by doping the polymer film to shift the operating window to lower applied potentials.<sup>[10]</sup> Oxygen can be blocked from the channel with oxygen-trapping additives<sup>[17]</sup> or by employing a secondary polymer layer with low oxygen permeability.<sup>[13]</sup> These methods are most effective for positive gate voltages as ORRs occur when the potential of the polymer is reducing (i.e., at a negative relative to Ag/AgCl). The second group

George G. Malliaras was an editor of this journal during the review and decision stage. For the MRS Communications policy on review and publication of manuscripts authored by editors, please refer to <http://www.mrs.org/editor-manuscripts/>.

of strategies improves stability by reducing the expansion of the amorphous regions of the film resulting from the injection and extraction of hydrated ions during (de)doping. This has been demonstrated previously by modifying the arrangement of polymer sidechains<sup>[18]</sup> and using additives.<sup>[17]</sup> These changes are particularly important at high doping levels (negative gate potentials) but also improve the cycling stability as the degree of active swelling is reduced. Another consideration in the stability of conducting polymer films is the removal of excess low molecular weight fraction which is usually done by soaking and can be enhanced by preconditioning.<sup>[19]</sup>

Most previous studies focus on stability of OECTs when operated over the full range of voltages to access the minimum in channel current and maximum in transconductance. However, many of the OECT-based bioelectronic devices do not require use across the full operational range. For example, biosensors<sup>[20]</sup> and neuromorphic devices<sup>[10]</sup> often leverage the near linear change in drain current in response to a change in gate potential which is only possible in the saturation regime.

In contrast, when large signal-to-noise is required and linearity is not important, the operation of OECTs in the subthreshold regime where the subthreshold slope ( $SS$ ) is maximized can be advantageous.<sup>[21]</sup> Thus, in most cases, OECTs do not need to operate across in both the saturation and subthreshold regimes simultaneously.

Here, we study the role of the applied gate voltage range on the stability of OECTs operated in 0.1 M aqueous NaCl with an Ag/AgCl gate electrode [Fig. 1(a)]. To understand whether the instability is material specific, we explore a range of polythiophene-based OMIECs including the most commonly used OMIEC, PEDOT:PSS [Fig. 1(b)], as well as a series of polythiophenes with varied side chain distributions,<sup>[18]</sup> p(g1T2-g5T2) [Fig. 1(c)], p(g2T2-g4T2) [Fig. 1(d)], and p(g3T2) [Fig. 1(e)]. The transfer characteristics show that PEDOT:PSS operates as a depletion-mode transistor, while the OMIECs operate as enhancement-mode devices [Fig. 1(f)]. Each device additionally displays hysteresis in the transfer characteristics where the forward and reverse sweeps are indicated by arrows.

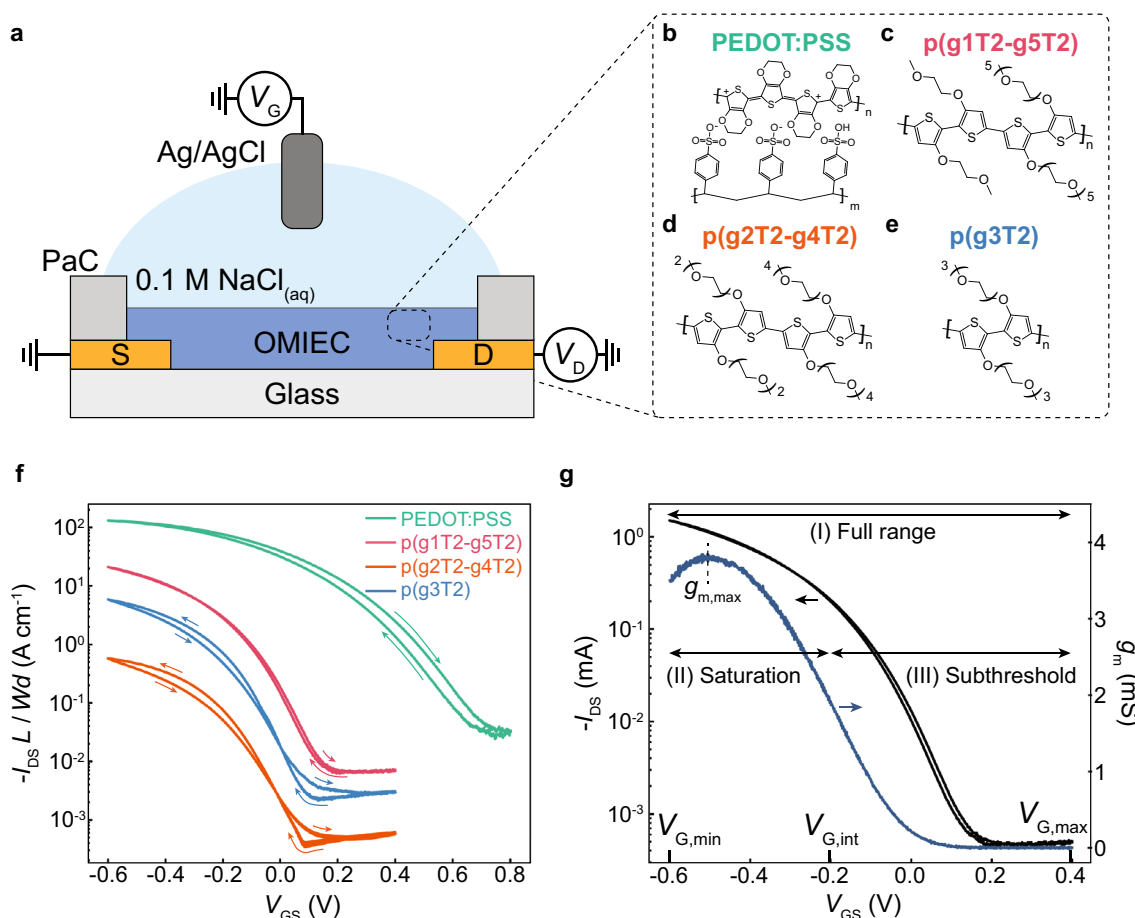


**Figure 1.** Stability testing of OECT channel materials. (a) Schematic drawing of an OECT structure. (b–e) Chemical structures of the studied channel OECT channel materials (b) PEDOT:PSS, (c) p(g1T2-g5T2), (d) p(g2T2-g4T2), and (e) p(g3T2). (f) Transfer curve measurements for the pristine devices for each OMIEC. The drain-source currents are normalized to the OECT geometry ( $Wd/L$ ) for comparison. Arrows denote the forward and reverse sweeps. (g) Operating regimes for OECTs used for stability testing consisting of (I) the full range ( $V_{G,min}$  to  $V_{G,max}$ ), (II) the saturation regime ( $V_{G,int}$  to  $V_{G,max}$ ), and (III) the subthreshold regime ( $V_{G,min}$  to  $V_{G,int}$ ).

We investigate the stability of each OEET in three different operating regimes: (I) the typical full OEET range ( $V_{GS}$  from  $-0.6$  to  $0.4$  V,  $-0.6$  to  $0.8$  V for PEDOT:PSS), (II) the saturation regime where the device is operated about the maximum transconductance ( $g_{m,max}$ ) ( $V_{GS}$  from  $-0.6$  to  $-0.2$  V,  $-0.6$  to  $0.0$  V for PEDOT:PSS), and (III) the subthreshold regime where the subthreshold slope is maximized ( $V_{GS}$  from  $-0.2$  to  $0.4$  V,  $0.0$  to  $0.8$  V for PEDOT:PSS) [Fig. 1(g)]. For all materials tested, we find that the channel is least stable when cycled across the full operating voltage range. This indicates that channel degradation is not specific to a particular voltage or the result of bias stress, but instead due to cycling between the on and off states.

## Materials and experiments

### Preparation of conducting polymer solutions

The PEDOT:PSS dispersion was prepared by mixing Clevis PH1000 (Heraeus) with 6%v/v ethylene glycol and 1%v/v (3-glycidyloxypropyl)trimethoxysilane (GOPS), sonicating for 10 min, and then filtering through a  $0.45\ \mu\text{m}$  polyvinylidene fluoride syringe filter. The solutions of p(g1T2-g5T2), p(g2T2-g4T2), and p(g3T2) were prepared by dissolving in chloroform ( $5\ \text{mg mL}^{-1}$ ) and stirring at room temperature overnight.

### Device fabrication

Fabrication of organic electrochemical transistors started with 10 min of sonication of borosilicate glass wafers ( $900\ \mu\text{m}$  thick, double-side polished Microchemicals) submerged in acetone followed by IPA then baked at  $150^\circ\text{C}$  to remove any residual moisture. Gold contacts are patterned using metal lift off which consisted of coating with AZ nLoF 2035 negative photoresist (Microchemicals) (spin coating at 500 RPM for 5 s, acceleration of  $1000\ \text{RPM s}^{-1}$ , followed by 3000 RPM for 45 s, acceleration of  $8000\ \text{RPM s}^{-1}$ , then soft baked at  $110^\circ\text{C}$  for 60 s) followed by UV exposure ( $60\ \text{mJ cm}^{-2}$ ), a post exposure bake ( $110^\circ\text{C}$  for 180 s), and development in AZ 726 MIF (Microchemicals) for 30 s. The patterned wafer was coated with 5 nm titanium then 100 nm gold (E-beam Evaporator, Kurt J. Lesker Company), and lift off was performed by submerging the wafer in acetone for 25 min followed by rinsing with acetone then IPA. The patterned metal-coated wafers are then coated with a parylene bilayer by first treating the wafer with oxygen plasma for 60 s followed by submerging the wafer in a dilute silane solution (3%v/v A174 silane dissolved in 0.1%v/v acetic acid in deionized water) for 45 s to improve parylene adhesion to the wafer. The silane-treated wafer is rinsed with ethanol and heated for 1 h at  $75^\circ\text{C}$  then coated with a  $2\ \mu\text{m}$  layer of parylene (PDS 2010 Labcoter 2, Specialty Coating Systems) followed by coating with a soap surfactant layer (2%v/v Micro 90 soap in deionized water spin-coated at 1000 RPM for 30 s and dried in air for 20 min) followed by a second deposition of a  $2\ \mu\text{m}$  layer of parylene. The trenches for depositing polymer channels are defined in the parylene bilayer

with photolithography by coating with AZ10XT positive resist (Microchemicals) (spin coating at 3000 RPM for 45 s, acceleration of  $8000\ \text{RPM s}^{-1}$ , soft bake at  $115^\circ\text{C}$  for 120 s) followed by UV exposure ( $540\ \text{mJ cm}^{-2}$ ) and developing in AZ 726 MIF developer (Microchemicals) for 10 min. Then, trenches are etched using reactive ion etching and the wafers were diced with a diamond scribe and tile cutter tool. Conducting polymers are spin-coated at 1000 RPM for 40 s. The resulting film thicknesses were  $218 \pm 56\ \text{nm}$ ,  $89 \pm 20\ \text{nm}$ ,  $129 \pm 22\ \text{nm}$ , and  $56 \pm 20\ \text{nm}$  for PEDOT:PSS, p(g1T2-g5T2), p(g2T2-g4T2), and p(g3T2), respectively. PEDOT:PSS coated wafers were baked at  $120^\circ\text{C}$  for 20 min for crosslinking of GOPS and soaked in deionized water overnight to remove excess PSS molecules. The conducting polymer channels are defined by peeling off the top parylene layer using Kapton tape, leaving conducting polymer only in the patterned trench. The channel width ( $W$ ) and length ( $L$ ) were  $W=400\ \mu\text{m}$ ,  $L=100\ \mu\text{m}$  for the PEDOT:PSS OEET,  $W=400\ \mu\text{m}$ ,  $L=50\ \mu\text{m}$  for the p(g1T2-g5T2), p(g2T2-g4T2), and p(g3T2) OEETs. A silicone well is defined using an adhesive-backed silicone (McMaster-Carr) to confine the electrolyte.

### Electrical characterization

Electrochemical transistors were characterized using a Keysight B2902A Source-Measure Unit controlled custom Python code. All experiments were performed using 0.1 M NaCl dissolved in water as the electrolyte and an Ag/AgCl pellet (2 mm diameter, 4 mm length) (World Precision Instruments) as the gate electrode. Cycling stability was tested using a constant sweep rate of  $0.2\ \text{V s}^{-1}$  and pulsing stability was tested by holding the device in the on and off states for 1 s each (pulse frequency of 0.5 Hz). Stability was tested for a single device of each material in the saturation regime first, followed by the subthreshold regime, and then the full range stability was tested last. Transconductance ( $g_m$ ) was calculated by taking the derivative of the drain current with respect to the gate voltage for the forward sweep of the transfer curve. The transfer curve was smoothed using a Savitzky–Golay filter in Python (window length of 53, polynomial order of 3) before taking the derivative to reduce the noise in the  $g_m$  curve. The subthreshold slope ( $SS$ ) was calculated as the inverse of the derivative of the logarithm of the drain current with respect to the gate voltage for the reverse sweep of the transfer curve. The transfer curve was smoothed using a Savitzky–Golay filter in Python (window length of 33, polynomial order of 3) before taking the derivative to reduce the noise in the  $SS$  curve. The maximum  $g_m$  and minimum  $SS$  were taken as the maximum and minimum values of the curves, respectively.

### Film thickness measurements

Film thicknesses were measured using a DekTak XT Profilometer with a scan rate of  $67\ \mu\text{m s}^{-1}$  and a stylus force of 1 mg. Each sample was measured in 6 locations and averaged.

## Results

The OECT materials in this study all display some degree of hysteresis in their transfer characteristics [Fig. 1(f)]. For both PEDOT:PSS and p(g1T2-g5T2), the magnitude of the forward sweep  $I_{DS}$  is always less than for the reverse sweep [Fig. 1(f)]. In contrast, the hysteresis for p(g2T2-g4T2) and p(g3T2) depends on the  $V_{GS}$  range. At positive gate biases, the forward sweep has a lower  $I_{DS}$  compared to the reverse sweep, but at negative gate biases, the forward sweep  $I_{DS}$  is much larger than that of the reverse sweep [Fig. 1(f)]. We attribute the hysteresis profile for p(g2T2-g4T2) and p(g3T2) to the energetics of filling hole sites. During the forward sweep, aggregated regions of the film dope first but have poor conduction due to their spatial separation.<sup>[22]</sup> Then, at high doping levels, bipolarons first occupy the amorphous regions leading to a substantial conductivity enhancement, but the generation of bipolarons in the aggregated regions leads to a decrease in the carrier transport properties.<sup>[23]</sup>

To examine the stability of the OECT channel materials, we adopted two different methodologies commonly used in the literature. First, we tested the stability of OECTs when cycled between the on and off state with a constant gate voltage sweep rate and a constant drain-source bias of  $V_{DS} = -0.6$  V (cycling stability).<sup>[17,19]</sup> The cycling stability yields transfer curves which can be used to derive the transconductance ( $g_m$ ) of the device by taking the derivative with respect to voltage. To quantify the transistor performance with increasing cycles, we use the maximum drain current ( $I_{DS,max}$ ) and the maximum transconductance ( $g_{m,max}$ ) for each cycle as figures of merit. To quantify stability, we compare  $I_{DS,max}$  and  $g_{m,max}$  to the values for the first cycle ( $I_{DS,max,0}$  and  $g_{m,max,0}$ , respectively).

During full range cycling stability tests, all channel materials show moderate decay in the  $g_{m,max}$  and  $I_{DS,max}$  over 100 cycles [Fig. 2(a)–(d)]. The PEDOT:PSS OECT is the most stable with a  $g_{m,max}$  and  $I_{DS,max}$  of 80% and 79% of their original

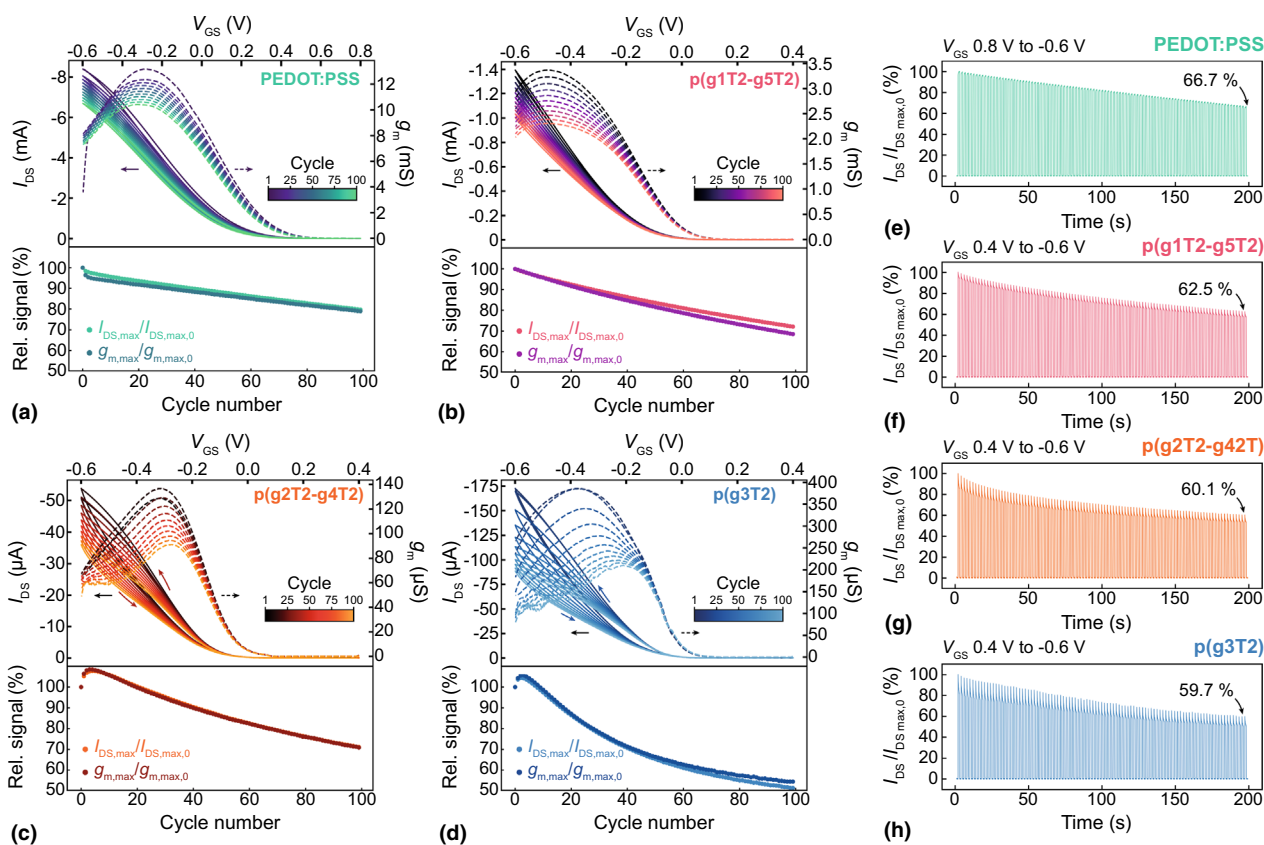


**Figure 2.** Full operating range OECT stability. Source-drain current ( $I_{DS}$ , solid lines, left y-axis) and transconductance ( $g_m$ , dashed lines, right y-axis) during OECT cycling (upper) and corresponding decay in the maximum current ( $I_{DS,max}$ ) and maximum transconductance ( $g_{m,max}$ ) (lower) for devices utilizing (a) PEDOT:PSS, (b) p(g1T2-g5T2), (c) p(g2T2-g4T2), and (d) p(g3T2) as channel materials. Each OECT is cycled 100 times between  $V_{min} = -0.6$  V, and  $V_{max} = 0.8$  V for PEDOT:PSS and 0.4 V for p(g1T2-g5T2), p(g2T2-g4T2), and p(g3T2), with the drain-source current ( $I_{DS}$ , solid lines, left y-axis) and transconductance ( $g_m$ , dashed lines, right y-axis) plotted for each 10th cycle.  $I_{DS,max}$  and  $g_{m,max}$  for each cycle are plotted as a percentage of the initial maximum current ( $I_{DS,max,0}$ ) and initial  $g_{m,max}$  ( $g_{m,max,0}$ ), respectively. The arrows in panels (c) and (d) indicate the forward and reverse voltage sweeps. Pulsing stability for OECTs utilizing (e) PEDOT:PSS, (f) p(g1T2-g5T2), (g) p(g2T2-g4T2), and (h) p(g3T2) channel materials. The source-drain current ( $I_{DS}$ ) is normalized to the maximum source-drain current of the first pulse ( $I_{DS,max,0}$ ).

values, respectively, after 100 cycles [Fig. 2(a)]. The  $V_{GS}$  corresponding to  $g_{m,max}$  also shifts slightly toward lower potentials. Similarly, the p(g1T2-g5T2) OECT has a decay in the  $I_{DS,max}$  and  $g_{m,max}$  to 72% and 69%, respectively, and shows little shift in the  $V_{GS}$  corresponding to  $g_{m,max}$ . Interestingly, the p(g2T2-g4T2) and p(g3T2) OECTs show an initial increase in both the  $I_{DS,max}$  and  $g_{m,max}$ , but the values quickly decay to 71% for p(g2T2-g4T2), and to 51% and 54%, respectively, for p(g3T2).

We also investigate the stability of OECTs when the channel is alternated between two gate voltages using pulses (pulsing stability) under a constant  $V_{DS} = -0.6$  V.<sup>[13,18]</sup> Here, we monitor the stability of  $I_{DS}$  as a percentage of the original maximum drain-source current ( $I_{DS,max,0}$ ) as the gate potential is alternated between  $-0.6$  and  $0.8$  V for PEDOT:PSS, and between  $-0.6$  and  $0.4$  V for the other materials. At the end of the series of pulses, we compare the maximum current of the last  $V_{GS}$  pulse to see the percentage decay of  $I_{DS}$ . All materials show a steady decay in the on-state  $I_{DS}$  with increased pulsing, and following

100 pulses, the  $I_{DS}$  is reduced to 67% for PEDOT:PSS and ca. 60% for the enhancement-mode materials.

In many OECT applications, the device does not need to be cycled between the fully off and fully on states. The saturation regime is where  $g_m$  peaks and thus yields the maximum changes in  $I_{DS}$  for small changes in  $V_{GS}$ . Operating near the peak in  $g_m$  is ideal for applications where a linear  $I_{DS}$  response to changes in  $V_{GS}$  is desired, such as biosensing, electrophysiology, and neuromorphic devices.<sup>[1,8,9]</sup> Additionally, operating in the saturation regime is necessary for applications where high currents (100  $\mu$ A up to 10 mA) are required. For saturation operation,  $I_{DS,max}$  and  $g_m$  are again the figures of merit to monitor for stability.

In contrast to full range cycling, the OECTs operated in the saturation regime all showed excellent stability. Following 100 cycles, the  $I_{DS,max}$  and  $g_{m,max}$  for the PEDOT:PSS remain at 100% and 98% of their original value, respectively, and the curves from different cycles overlap with one another [Fig. 3(a)]. The performance of the p(g1T2-g5T2) transistor

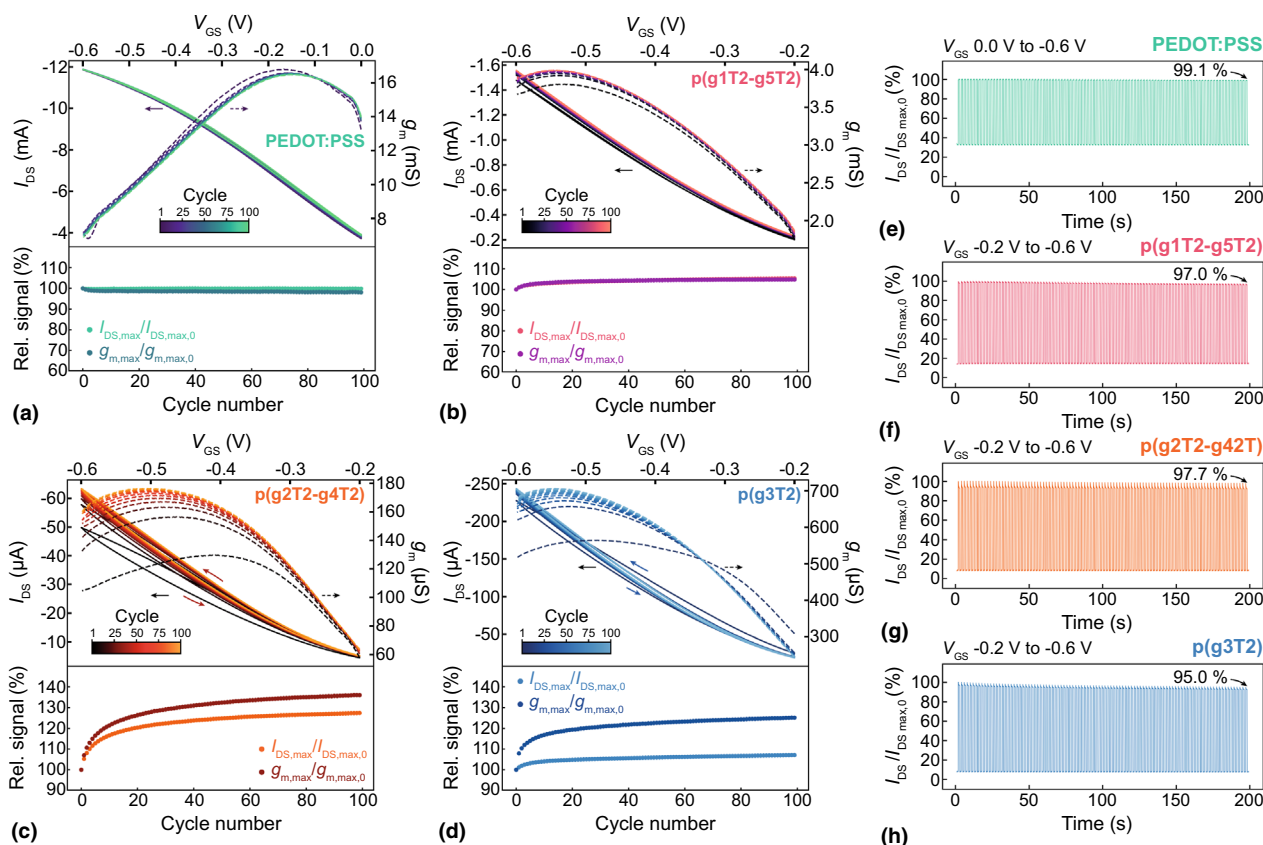


**Figure 3.** Saturation regime OECT stability. Source-drain current ( $I_{DS}$ , solid lines, left y-axis) and transconductance ( $g_m$ , dashed lines, right y-axis) during OECT cycling (upper) and corresponding decay in the maximum current ( $I_{DS,max}$ ) and maximum transconductance ( $g_{m,max}$ ) (lower) for devices utilizing (a) PEDOT:PSS, (b) p(g1T2-g5T2), (c) p(g2T2-g4T2), and (d) p(g3T2) channel materials. Each OECT is cycled 100 times between  $V_{min} = -0.6$  V, and  $V_{max} = 0.0$  V for PEDOT:PSS and  $-0.2$  V for p(g1T2-g5T2), p(g2T2-g4T2), and p(g3T2), with the drain-source current ( $I_{DS}$ , solid lines, left y-axis) and transconductance ( $g_m$ , dashed lines, right y-axis) plotted for each 10th cycle.  $I_{DS,max}$  and  $g_{m,max}$  for each cycle are plotted as a percentage of the initial maximum current ( $I_{DS,max,0}$ ) and initial transconductance ( $g_{m,max,0}$ ), respectively. Pulsing stability for OECTs utilizing (e) PEDOT:PSS, (f) p(g1T2-g5T2), (g) p(g2T2-g4T2), and (h) p(g3T2) channel materials. The source-drain current ( $I_{DS}$ ) is normalized to the maximum source-drain current of the first pulse ( $I_{DS,max,0}$ ).

improved slightly with cycling, with a final  $I_{DS,max}$  and  $g_{m,max}$  of 105% of their original values [Fig. 3(b)]. Surprisingly, the performance of both the p(g2T2-g4T2) and p(g3T2) OECTs improves substantially over 100 cycles with  $I_{DS,max}$  and  $g_{m,max}$  increasing to 127% and 136%, respectively, for p(g2T2-g4T2) and to 107% and 125%, respectively, for p(g3T2) [Fig. 3(c)–(d)]. All channel materials are stable during pulsing in the saturation regime, retaining 95% or more of the original  $I_{DS}$ .

Based on previous reports,<sup>[15]</sup> we expect that the largest reversible mass uptake (and therefore degree of swelling) occurs in the saturation regime where the modulation of the carrier density is largest. Thus, we would expect degradation due to swelling/deswelling of the material would be present in this  $V_{GS}$  range. However, the increase in performance for the p(g2T2-g4T2) and p(g3T2) OECTs suggests that some degree of reversible swelling can be beneficial for device performance. The reversible swelling and increasing solvation may allow chains to rearrange, improving tie-chain connections between aggregated regions or increasing ion conductivity, allowing for higher carrier densities to be reached for the same gate potential.<sup>[16]</sup> This result partially contradicts the hypothesis that a high degree of active swelling is responsible for the instability.<sup>[16,18]</sup> The high stability of the devices in the saturation regime also indicates that charging to high carrier densities does not necessarily cause instability from overoxidation.

In applications where low power consumption and high signal-to-noise ratios are critical, subthreshold operation of OECTs is most practical.<sup>[11,21]</sup> The subthreshold regime yields the sharpest relative change in  $I_{DS}$  with respect to small changes in  $V_{GS}$ . OECTs exhibit relatively high subthreshold swing, approaching the thermodynamic limit of silicon devices ( $60 \text{ mV dec}^{-1}$ ).<sup>[11,21]</sup> OECTs operated in the subthreshold regime could be of potential use for potentiometric sensors which have a logarithmic relationship between concentration and potential output (i.e., ion-selective OECTs<sup>[20]</sup> and enzymatic sensors<sup>[24]</sup>) to achieve a linear response. For subthreshold operation, we again use the maximum current as one of the figures of merit. However, instead of using  $g_{m,max}$  which is relevant when operating in the linear regime, we use the minimum subthreshold slope ( $SS_{min}$ ) as a figure of merit for subthreshold operation. Furthermore, to quantify instability in subthreshold performance, we divide the initial subthreshold slope ( $SS_{min,0}$ ) by the  $SS_{min}$  for each cycle. This quantification yields a percentage of  $<100\%$  when  $SS_{min}$  increases, thereby decreasing the performance of the OECT.

The PEDOT:PSS OECT appears unstable when operated in the subthreshold regime [Fig. 4(a)] with the maximum current at  $V_{GS}=0 \text{ V}$  dropping to 50% of the original value after 100 cycles. However, the  $SS_{min}$  is only slightly larger after cycling ( $SS_{min,0}/SS_{min}=96\%$ ), indicating that the decrease in  $I_{DS}$  results from a shift in the transfer characteristics to lower voltages rather than a decay in the electronic transport properties of the channel. Previous reports show that PEDOT:PSS produces

$\text{H}_2\text{O}_2$  when reduced,<sup>[14]</sup> and that the production of  $\text{H}_2\text{O}_2$  can shift the pH of the aqueous electrolyte.<sup>[13]</sup> From these two reports, we hypothesize that the shift in the transfer characteristics of PEDOT:PSS during subthreshold cycling may be due to shifts in the electrolyte pH.<sup>[25]</sup>

In contrast to PEDOT:PSS, p(g1T2-g5T2), p(g2T2-g4T2), and p(g3T2) all are highly stable when operated in the subthreshold regime [Fig. 4(b)–(d)]. Furthermore, they all have much better subthreshold performance than PEDOT:PSS ( $SS_0 = 133 \text{ mV dec}^{-1}$ ) with  $SS_0$  of 82, 101, and 90  $\text{mV dec}^{-1}$ , for p(g1T2-g5T2), p(g2T2-g4T2), and p(g3T2) OECTs, respectively. The p(g1T2-g5T2) OECT shows no degradation in its performance after 100 cycles in the subthreshold regime, with a final  $I_{DS,max}$  of 104% and  $SS_{min,0}/SS_{min}$  of 101%. The  $I_{DS,max}$  for p(g2T2-g4T2) and p(g3T2) increase to 112 and 184% of  $I_{DS,max,0}$ , respectively, following 100 cycles, showing a similar enhancement in drain-source current as when the OECTs are cycled in the saturation regime. The  $SS$  for p(g2T2-g4T2) stays roughly the same following cycling ( $SS_{min,0}/SS_{min} = 103\%$ ) and is enhanced for p(g3T2) ( $SS_{min,0}/SS_{min} = 115\%$ ). Since the enhancement in  $SS$  observed for p(g3T2) only occurs over the first 5–10 cycles, we expect that it may be related to a slow equilibration process which occurs when switching operation from the saturation regime to the subthreshold regime.

## Discussion

Our results show that OECTs utilizing the polythiophene OMIEC channels studied here are least stable when operated over the full range of voltages, or in other words, when the device is repeatedly cycled from the fully off state to the peak in transconductance (Figure S1). Furthermore, by separately testing the saturation regime and subthreshold regime stability, we conclude that there is no specific gate voltage range which is responsible for the degradation in performance. Instead, the decay in OECT performance during operation is primarily due to effects related to transitioning from the highly oxidized (on) state and the highly reduced (off) state or vice versa. While the root cause of the instability is not addressed in this work, we believe the results here provide a framework for utilizing OECTs while avoiding instability in the device response.

Our findings help narrow the potential causes for instability in OECTs, as often operation in or to a particular voltage regime is cited as the root cause for degradation of the channel. For the electrochemical degradation process, it is possible that reactive oxygen species are produced at positive gate biases, but these species only react with the highly oxidized polymer.<sup>[13]</sup> If the lifetime of the reactive oxygen species is sufficiently short, the degradation will only occur when the device is quickly cycled from the ORR potential to the highly oxidized state. For structural degradation, our results indicate that swelling/deswelling alone does not degrade the channel given that OECTs show high stability in the saturation regime. Instead, the transition between the highly oxidized state and the highly reduced state is the main driver of instability.

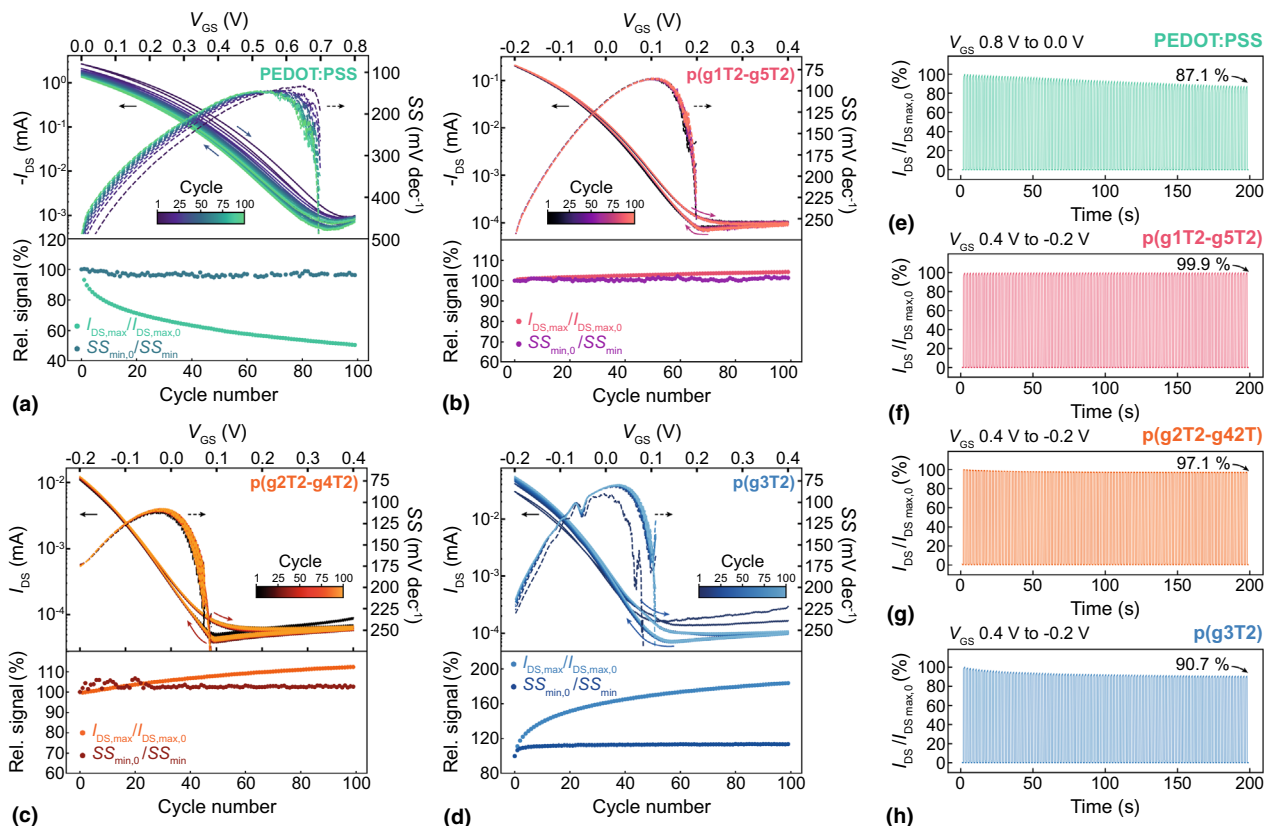


**Figure 4.** Subthreshold regime OECT stability. Cycling stability (upper) and corresponding decay in the maximum current ( $I_{DS,max}$ ) and minimum subthreshold slope ( $SS_{min}$ ) (lower) for OECTs utilizing (a) PEDOT:PSS, (b) p(g1T2-g5T2), (c) p(g2T2-g4T2), and (d) p(g3T2) channel materials. Each OECT is cycled 100 times between  $V_{min}$ , 0.0 V and  $V_{max}$ , 0.8 V for PEDOT:PSS, and  $V_{min}$ , -0.2 V and  $V_{max}$ , 0.4 V for p(g1T2-g5T2), p(g2T2-g4T2), and p(g3T2), with the drain-source current ( $I_{DS}$ , solid lines, left y-axis) and subthreshold slope (SS, dashed lines, right y-axis) plotted for each 10th cycle.  $I_{DS,max}$  and  $SS_{min}$  are plotted as a percentage of the initial maximum current ( $I_{DS,max,0}$ ) and initial subthreshold slope ( $SS_{min,0}$ ), respectively. Pulsing stability for OECTs utilizing (e) PEDOT:PSS, (f) p(g1T2-g5T2), (g) p(g2T2-g4T2), and (h) p(g3T2) channel materials. The source-drain current ( $I_{DS}$ ) is normalized to the maximum source-drain current of the first pulse ( $I_{DS,max,0}$ ).

In our cycling stability tests, we observe a hysteresis between the forward and reverse sweeps which is quite large when the OECTs are cycled across the full voltage range but is reduced substantially in the reduced range cycling, similar to previous observations.<sup>[30]</sup> The correlation between the degradation and the hysteresis brings up the question if the two processes are related. For example, the increased charge density on the polymer backbone during oxidation may enhance the enthalpic interactions between the polar solvent and charged backbone, thereby increasing the energy required to return the reduced state. The polar solvent-polymer interactions during solvation and desolvation of chains could additionally break some of the weaker  $\pi$ - $\pi$  interactions and add additional disorder to the aggregated regions<sup>[16]</sup> or slowly solubilize the channel into the aqueous electrolyte. Thus, we hypothesize the structural degradation may be the accumulation of irreversible reorganizations of polymer chains in addition to the parasitic electrochemical reactions with reactive oxygen species.

One interesting result is the enhancement in performance for p(g2T2-g4T2) and p(g3T2) OECTs when cycled in either

the saturation or subthreshold regimes. While the mechanism for this conductivity enhancement is not clear from our results alone, we discuss some of the possible mechanisms which could cause this enhancement. First, during reversible cycling, some anions, which are charge-compensated by holes on the polymer backbone, may remain in the film after each cycle.<sup>[26]</sup> These trapped anion-hole pairs can then shift the effective potential of the OMIEC channel and cause retention of water, which hydrates the anion. Over the course of repeated cycling, the channel typically accumulates excess water carried in by ions, where most of the excess water remains in the amorphous regions of the polymer<sup>[27]</sup> and could thus improve ion conductivity through the material in following cycles. The excess water may also solubilize individual polymer chains and allow them to rearrange, possibly bridging conductive aggregated regions.<sup>[16]</sup> Finally, added water may screen charge-charge interactions and lower the energy for bipolarons to form in the disordered regions of the film, where bipolarons in disordered regions have been shown to notably enhance the electrical conductivity.<sup>[23]</sup>

OECTs are increasingly leveraged to measure, amplify, and compute bioelectronic signals on-site. The goal of these works is to develop tools for human health monitoring, often with life-saving implications ranging from COVID-19 detection<sup>[7]</sup> to monitoring epileptic<sup>[28]</sup> seizures. However, any tool which may influence a patient's diagnosis or treatment must produce a stable output signal for patient safety and treatment efficacy. While we show that OECTs are unstable when cycled over large gate voltage ranges, this study demonstrates that devices are generally robust to cycling within either the saturation or subthreshold regimes. The findings presented here should be considered to ensure high measurement precision and reliability in these critical healthcare applications. For example, one method of OECT biosensing is to measure subtle shifts in the transfer response, which has been reported to indicate sensitivity for picomolar analyte concentrations.<sup>[29]</sup> Our results suggest that these measurements, which were taken over the full operating range, may be prone to cyclic instability, making it difficult to differentiate between shifts due to the biomarker and due to instability. In this case, alternate techniques, or saturation regime limited operation, should be considered to ensure accurate measurement. In contrast, the use of OECTs for electrophysiology<sup>[1,28]</sup> only requires a limited operating voltage window near the peak in transconductance (i.e., saturation regime), meeting the criteria for the stable operation that is desired for prolonged neuroelectronic measurements. In some cases, the sharp change in conductivity in the subthreshold regime is needed to enhance the signal-to-noise for feature detection in electrophysiology<sup>[21]</sup> or complementary inverters.<sup>[11]</sup> Our results suggest that OECTs can be utilized in the subthreshold regime with high stability with the caveat that gate potentials driving high doping densities should be avoided. The results from this work help to elucidate the specific pathways causing degradation in the performance of OECT channel materials, which can be leveraged to find new ways of engineering more stable devices for high-performance bioelectronic tools.

## Acknowledgments

The authors would like to thank Lukas Bongartz for the fruitful discussions.

## Author contributions

STK conceived the research, designed the experiments, fabricated the samples, analyzed the data, and wrote the original manuscript draft. MM synthesized p(g1T2-g5T2), p(g2T2-g4T2), and p(g3T2) under the supervision of IM. STK, LWG, SLB, and GGM wrote the manuscript with input from all authors.

## Funding

S.T.K. gratefully acknowledges funding from the European Union's Horizon 2020 research and innovation program under the Marie Skłodowska-Curie grant agreement 101022365. L.W.G. gratefully acknowledges funding from the Engineering and Physical Sciences Research Council (UK) Doctoral Training Partnership (Grant EP/W524633/1). S.L.B. acknowledges funding from the Cambridge International & Churchill Pocho-bradsky Scholarship. S.T.K., I.M., and G.G.M. acknowledge support from the Engineering and Physical Sciences Research Council (UK) (Grant EP/W017091/1).

## Data availability

All data for the work are either included in this manuscript or are part of the Electronic Supplementary Information file. The datasets generated during and/or analyzed during the current study are available from the corresponding author upon reasonable request.

## Declarations

### Conflict of interest

The authors declare no conflicts of interest.

## Rights retention statement

This work was funded by the UKRI. For the purpose of open access, the author has applied a Creative Commons Attribution (CC BY) license to any Author Accepted Manuscript version arising.

## Supplementary Information

The online version contains supplementary material available at <https://doi.org/10.1557/s43579-023-00511-6>.

## Open Access

This article is licensed under a Creative Commons Attribution 4.0 International License, which permits use, sharing, adaptation, distribution and reproduction in any medium or format, as long as you give appropriate credit to the original author(s) and the source, provide a link to the Creative Commons licence, and indicate if changes were made. The images or other third party material in this article are included in the article's Creative Commons licence, unless indicated otherwise in a credit line to the material. If material is not included in the article's Creative Commons licence and your intended use is not permitted by statutory regulation or exceeds the permitted use, you will need to obtain permission directly from the copyright holder. To view a copy of this licence, visit <http://creativecommons.org/licenses/by/4.0/>.



## References

1. Y. Zhong, A. Saleh, S. Inal, Decoding electrophysiological signals with organic electrochemical transistors. *Macromol. Biosci.* **21**, 2100187 (2021)
2. S.L. Bidinger, S.T. Keene, S. Han, K.W. Plaxco, G.G. Malliaras, T. Hasan, Pulsed transistor operation enables miniaturization of electrochemical aptamer-based sensors. *Sci. Adv.* **8**, eadd4111 (2022)
3. S.T. Keene, C. Lubrano, S. Kazemzadeh, A. Melianas, Y. Tuchman, G. Polino, P. Scognamiglio, L. Cinà, A. Salleo, Y. Van De Burgt, F. Santoro, A biohybrid synapse with neurotransmitter-mediated plasticity. *Nat. Mater.* **19**, 969 (2020)
4. D. Khodagholy, J. Rivnay, M. Sessolo, M. Gurfinkel, P. Leleux, L.H. Jimison, E. Stavrinidou, T. Herve, S. Sanaur, R.M. Owens, G.G. Malliaras, High transconductance organic electrochemical transistors. *Nat. Commun.* **4**, 2133 (2013)
5. F. Santoro, Y. Van De Burgt, S.T. Keene, B. Cui, A. Salleo, Enhanced cell-chip coupling by rapid femtosecond laser patterning of soft PEDOT:PSS biointerfaces. *ACS Appl. Mater. Interfaces* **9**, 39116 (2017)
6. S.T. Keene, V. Gueskine, M. Berggren, G.G. Malliaras, K. Tybrandt, I. Zozoulenko, Exploiting mixed conducting polymers in organic and bioelectronic devices. *Phys. Chem. Chem. Phys.* **24**, 19144 (2022)
7. K. Guo, S. Wustoni, A. Koklu, E. Díaz-Galicia, M. Moser, A. Hama, A.A. Alqahtani, A.N. Ahmad, F.S. Alhamlan, M. Shuaib, A. Pain, I. McCulloch, S.T. Arold, R. Grünberg, S. Inal, Rapid single-molecule detection of COVID-19 and MERS antigens via nanobody-functionalized organic electrochemical transistors. *Nat. Biomed. Eng.* **5**, 666 (2021)
8. D. Ohayon, G. Nikiforidis, A. Savva, A. Giugni, S. Wustoni, T. Palanisamy, X. Chen, I.P. Maria, E. Di Fabrizio, P.M.F.J. Costa, I. McCulloch, S. Inal, Biofuel powered glucose detection in bodily fluids with an n-type conjugated polymer. *Nat. Mater.* **19**, 456 (2020)
9. E.J. Fuller, S.T. Keene, A. Melianas, Z. Wang, S. Agarwal, Y. Li, Y. Tuchman, C.D. James, M.J. Marinella, J.J. Yang, A. Salleo, A.A. Talin, Parallel programming of an ionic floating-gate memory array for scalable neuromorphic computing. *Science* **364**, 570 (2019)
10. S.T. Keene, A. Melianas, Y. Van De Burgt, A. Salleo, Mechanisms for enhanced state retention and stability in redox-gated organic neuromorphic devices. *Adv. Electron. Mater.* **5**, 1800686 (2019)
11. W. Huang, J. Chen, Y. Yao, D. Zheng, X. Ji, L.-W. Feng, D. Moore, N.R. Glavin, M. Xie, Y. Chen, R.M. Pankow, A. Surendran, Z. Wang, Y. Xia, L. Bai, J. Rivnay, J. Ping, X. Guo, Y. Cheng, T.J. Marks, A. Facchetti, Vertical organic electrochemical transistors for complementary circuits. *Nature* **613**, 496 (2023)
12. H. Sun, M. Vagin, S. Wang, X. Crispin, R. Forchheimer, M. Berggren, S. Fabiano, Complementary logic circuits based on high-performance n-type organic electrochemical transistors. *Adv. Mater.* **30**, 1704916 (2018)
13. S. Zhang, P. Ding, T.-P. Ruoko, R. Wu, M.-A. Stoeckel, M. Massetti, T. Liu, M. Vagin, D. Meli, R. Kroon, J. Rivnay, S. Fabiano, Toward stable p-type thiophene-based organic electrochemical transistors. *Adv. Funct. Mater.* **33**, 2302249 (2023)
14. A. Giovannitti, R.B. Rashid, Q. Thiburce, B.D. Paulsen, C. Cendra, K. Thorley, D. Moia, J.T. Mefford, D. Hanifi, D. Weiyuan, M. Moser, A. Salleo, J. Nelson, I. McCulloch, J. Rivnay, Energetic control of redox-active polymers toward safe organic bioelectronic materials. *Adv. Mater.* **32**, 1908047 (2020)
15. A. Savva, C. Cendra, A. Giugni, B. Torre, J. Surgailis, D. Ohayon, A. Giovannitti, I. McCulloch, E. Di Fabrizio, A. Salleo, J. Rivnay, S. Inal, Influence of water on the performance of organic electrochemical transistors. *Chem. Mater.* **31**, 927 (2019)
16. G. LeCroy, C. Cendra, T.J. Quill, M. Moser, R. Hallani, J.F. Ponder, K. Stone, S.D. Kang, A.Y.-L. Liang, Q. Thiburce, I. McCulloch, F.C. Spano, A. Giovannitti, A. Salleo, Role of aggregates and microstructure of mixed-ionic-electronic-conductors on charge transport in electrochemical transistors. *Mater. Horiz.* **10**, 2568 (2023)
17. T.C. Hidalgo Castillo, M. Moser, C. Cendra, P.D. Nayak, A. Salleo, I. McCulloch, S. Inal, Simultaneous performance and stability improvement of a p-type organic electrochemical transistor through additives. *Chem. Mater.* **34**, 6723 (2022)
18. M. Moser, T.C. Hidalgo, J. Surgailis, J. Gladisch, S. Ghosh, R. Sheelamantula, Q. Thiburce, A. Giovannitti, A. Salleo, N. Gasparini, A. Wadsworth, I. Zozoulenko, M. Berggren, E. Stavrinidou, S. Inal, I. McCulloch, Side chain redistribution as a strategy to boost organic electrochemical transistor performance and stability. *Adv. Mater.* **32**, 2002748 (2020)
19. S.L. Bidinger, S. Han, G.G. Malliaras, T. Hasan, Highly stable PEDOT:PSS electrochemical transistors. *Appl. Phys. Lett.* **120**, 0079011 (2022)
20. S. Han, S. Yamamoto, A.G. Polyravas, G.G. Malliaras, Microfabricated ion-selective transistors with fast and super-Nernstian response. *Adv. Mater.* **32**, 2004790 (2020)
21. V. Venkatraman, J.T. Friedlein, A. Giovannitti, I.P. Maria, I. McCulloch, R.R. McLeod, J. Rivnay, Subthreshold operation of organic electrochemical transistors for biosignal amplification. *Adv. Sci.* **5**, 1800453 (2018)
22. S.T. Keene, J.E.M. Laulainen, R. Pandya, M. Moser, C. Schnedermann, P.A. Midgley, I. McCulloch, A. Rao, G.G. Malliaras, Hole-limited electrochemical doping in conjugated polymers. *Nat. Mater.* **22**, 1121 (2023)
23. P. Cavassin, I. Holzer, D. Tsokkou, O. Bardagot, J. Réhault, N. Banerji, Electrochemical doping in ordered and disordered domains of organic mixed ionic-electronic conductors. *Adv. Mater.* **35**, 2300308 (2023)
24. S.T.M. Tan, A. Giovannitti, A. Melianas, M. Moser, B.L. Cotts, D. Singh, I. McCulloch, A. Salleo, High-gain chemically gated organic electrochemical transistor. *Adv. Funct. Mater.* **31**, 2010868 (2021)
25. G. Scheiblin, R. Coppard, R.M. Owens, P. Mailley, G.G. Malliaras, Referenceless pH sensor using organic electrochemical transistors. *Adv. Mater. Technol.* **2**, 1600141 (2017)
26. R. Wu, B.D. Paulsen, Q. Ma, I. McCulloch, J. Rivnay, Quantitative composition and mesoscale ion distribution in p-type organic mixed ionic-electronic conductors. *ACS Appl. Mater. Interfaces* **15**, 30553 (2023)
27. L.Q. Flagg, L.E. Asselta, N. D'Antona, T. Nicolini, N. Stingelin, J.W. Onorato, C.K. Luscombe, R. Li, L.J. Richter, In situ studies of the swelling by an electrolyte in electrochemical doping of ethylene glycol-substituted polythiophene. *ACS Appl. Mater. Interfaces* **14**, 29052 (2022)
28. D. Khodagholy, T. Doublet, P. Quilichini, M. Gurfinkel, P. Leleux, A. Ghestem, E. Ismailova, T. Hervé, S. Sanaur, C. Bernard, G.G. Malliaras, In vivo recordings of brain activity using organic transistors. *Nat. Commun.* **4**, 1575 (2013)
29. Y. Liang, C. Wu, G. Figueroa-Miranda, A. Offenhäusser, D. Mayer, Amplification of aptamer sensor signals by four orders of magnitude via interdigitated organic electrochemical transistors. *Biosens. Bioelectron.* **144**, 111668 (2019)
30. R. Shameem, L.M. Bongartz, A. Weissbach, H. Kleemann, K. Leo, Hysteresis in organic electrochemical transistors: relation to the electrochemical properties of the semiconductor. *Appl. Sci.* **13**, 5754 (2023). <https://doi.org/10.3390/app13095754>

**Publisher's Note** Springer Nature remains neutral with regard to jurisdictional claims in published maps and institutional affiliations.